Phys. Status Solidi B **248**, No. 10, 2213–2221 (2011) / **DOI** 10.1002/pssb.201147121

physica status solidi b
www.pss-b.com
basic solid state physics

From electrons to materials

Feature Article

Thomas Hammerschmidt, Georg K. H. Madsen, Jutta Rogal, and Ralf Drautz*

ICAMS, Ruhr-Universität Bochum, 44801 Bochum, Germany

Received 4 March 2011, revised 14 May 2011, accepted 16 May 2011
Published online 24 June 2011

Dedicated to Manfred Fähnle on the occasion of his 60th birthday

Keywords bond-order potentials, density functional theory, rare-event dynamics, tight-binding method

* Corresponding author: e-mail ralf.drautz@icams.rub.de, Phone: +49 234 3229308, Fax: +49 234 3214977

In this article, we discuss how microstructural length and time scales may be reached in atomistic simulations. We bridge from electronic properties to properties of materials by employing a systematic coarse graining of the electronic structure to effective interatomic interactions. In combination with extended time scale simulations the elementary processes of microstructural evolution may then be described. We present our approach to the derivation of tight-binding models from density functional theory, the characterization of the interatomic interaction using bond-order potentials and extended time scale simulations based on adaptive kinetic Monte Carlo. Applications to structural stability in iron, internal interfaces in tungsten and hydrogen diffusion in iron are discussed briefly and relate our approach to Manfred Fähnle's work.

1 Introduction The calculation of thermodynamic and kinetic properties from Hamiltonians that are based on first principles calculations represents an overarching theme in the many contributions of Manfred Fähnle's research. In a recent paper Manfred Fähnle gave an overview of the activties of his group on modelling thermodynamic properties based on first principles [1]. Within the framework of the cluster expansion method [2] an accurate description of the energy within density functional theory is mapped on a lattice gas Hamiltonian. The model is fully characterized by only a few cluster expansion coefficients and the occupation of the lattice sites with different atomic species. This makes it possible to use standard enumeration and Monte Carlo or Cluster Variation methods to search for new ground states and to calculate phase diagrams from first principles [3–6].

While the examples presented in Ref. [1] in particular exploit the dramatic simplification that is possible when atoms occupy the regular positions of a crystal lattice, for many atomic processes in materials the assumption of a simple crystal lattice cannot be justified. For example, often the underlying lattice changes during phase transformations. Dislocations, grain boundaries and interfaces are important for the mechanical properties of a material but often are difficult to model on a lattice. Diffusion may involve concerted and counterintuitive displacements of many atoms that cannot be readily described on a simple lattice.

The generalization of the cluster expansion away from regular crystal lattices is possible (see, for example [7]), but the resulting formal many-atom expansion converges only slowly and is hardly feasible for multi-component systems. Therefore the conceptual simplicity of the cluster expansion method is lost when one tries to extend it to an off-lattice expansion, making it a fitting approach that requires the numerical determination of a vast number of parameters. Instead, a physically intuitive and better convergent expansion is required that makes use of the properties of the underlying electronic structure. As in general the electronic structure is complex, simplifications need to be made to obtain a more straightforward interpretation of the electronic structure, of course at an expense of accuracy compared to lattice-based cluster expansion approaches. The simplification and analysis of the electronic structure within the tight-binding (TB) approximation therefore represents another important cornerstone of Manfred Fähnle's research [8, 9]. TB models are sufficiently simple such that the effective interaction between atoms may be characterized using a moments expansion within the framework of analytic bond-order potentials (BOPs). By combining, for example, BOPs with extended time scale simulations such as adaptive kinetic Monte Carlo (akMC), atomistic simulations may be carried out that reach length and time scales that are suitable for bridging to a microstructural description.

In this contribution we summarize three consecutive steps that aim at a systematic and physically intuitive coarse graining of the length and time scales from electrons to materials,

1. Tight-binding models: TB models are obtained by systematically simplifying the electronic structure within density functional theory by first representing the electronic structure within an optimized atom-centred minimal basis and subsequent interpolation of the resulting matrix elements,
2. Bond-order potentials: analytic BOPs are derived by approximating the density matrix, the local atomic density of states and local atomic energy using a moments expansion. Within bond-order potential theory, the electronic structure is only implicitly present, the BOPs are effective interatomic potentials that are derived from the electronic structure,
3. Adaptive kinetic Monte Carlo: the akMC method is applied to bridge the time scale of atomic vibrations in a solid to the time scale of atomic diffusion, which governs the time scale of microstructural changes in a material.

The outline of the paper is as follows. In Section 2, we present the tight-binding approximation and discuss how the required parameters are obtained from density functional theory (DFT). An application of TB to iron is discussed briefly. In Section 3, the derivation of bond-order potentials from the TB approximation is summarized and the application of BOPs in molecular dynamics (MD) simulations of tungsten is illustrated. In Section 4, rare event dynamics is introduced with a special focus on adaptive kinetic Monte Carlo. The application of akMC to diffusion of hydrogen in iron is discussed.

2 Tight-binding approximation from density functional theory

The TB approximation may be formally introduced as a second-order expansion of the density functional energy [10] in charge and magnetic fluctuations with respect to the overlapping charge densities of charge neutral, non-magnetic free atoms [11–15]. As the TB model is obtained directly from DFT, the functional form and the parameters of the model may also be fully characterized from DFT. We here summarize how a d-valent TB model for iron may be constructed [16]. If we assume that the atoms remain charge neutral, the TB energy functional may be written as

$$E_{\mathrm{TB}} = E_{\mathrm{bond}} + E_{\mathrm{rep}} + E_{\mathrm{emb}} + E_{\mathrm{mag}} - E_{\text{free-atoms}}. \tag{1}$$

The first term is the bond energy of the d-electrons within the TB bond model [11] which will be outlined in the following. The next two terms are interatomic potentials that will be described in Section 2.2. The term E_{mag} describes the Stoner exchange energy,

$$E_{\mathrm{mag}} = -\frac{1}{4}\sum_{J} I_J m_J^2, \tag{2}$$

with the magnetic moment m_J on atom J and the Stoner exchange integral I_J. The term $E_{\text{free-atoms}}$ corresponds to the energy of the charge neutral, non-magnetic atoms at infinite separation.

2.1 Optimal atomic orbital bond energy The first term of Eq. (1) corresponds to the bond energy of the d-electrons within the TB bond model [11, 17],

$$E_{\mathrm{bond}} = \sum_{\sigma=\uparrow,\downarrow} \sum_{\substack{I\mu J\nu \\ I\neq J}} \rho^{\sigma}_{I\mu J\nu} H_{I\mu J\nu}, \tag{3}$$

where $H_{I\mu J\nu} = \langle \varphi_{I\mu} | \hat{H} | \varphi_{J\nu} \rangle$ corresponds to the Hamiltonian matrix elements between orbitals μ and ν on atoms I and J and ρ^{σ} is the density matrix of the up-spin ($\sigma = \uparrow$) and down-spin ($\sigma = \downarrow$) channel. Following the work of Fähnle, Meyer, Elsässer and co-workers [18, 19] we have recently introduced a numerically efficient method for obtaining the TB matrix elements directly from density functional calculations [16]. The method is based on downfolding a multiple-ζ atomic orbital basis to a minimal basis, $\{|\varphi_{I\mu}\rangle\}$. The downfolding is done by maximizing the projection P of the occupied orbital wavefunctions ψ_n on the minimal basis

$$P_n = \sum_{I\mu J\nu} \langle \psi_n | \varphi_{I\mu} \rangle S^{-1}_{I\mu J\nu} \langle \varphi_{J\nu} | \psi_n \rangle, \tag{4}$$

$$P = N_e^{-1} \sum_n f_n P_n, \tag{5}$$

where f_n is the occupation of the eigenstate n, N_e the number of valence electrons and S the overlap matrix $S_{I\mu J\nu} = \langle \varphi_{I\mu} | \varphi_{J\nu} \rangle$.

Using a symmetric Löwdin procedure to orthogonalize the minimal basis Hamiltonian and rotating each of the 6×6 sub-matrices of the sd-minimal basis LCAO-Hamilton $H_{I\mu J\nu}$ and overlap $S_{I\mu J\nu}$ matrices into a bond-oriented coordinate system, we obtain the ssσ, sdσ, ddσ, ddπ and ddδ bond integrals [16] in the two-center approximation [20]. In our orthogonal d-valent TB model we retain only the ddσ, ddπ and ddδ integrals. For a given interatomic distance we found these bond integrals to be transferable between close-packed structures and the atomic dimer. Furthermore we found that they could be well parameterized by simple exponentials as

$$\beta_{\mathrm{dd}\lambda}(R) = a_{\mathrm{dd}\lambda} \exp(-b_{\mathrm{dd}\lambda} R), \quad \lambda = \sigma, \pi, \delta. \tag{6}$$

The bond integrals obtained here are compared to those of two other orthogonal TB models in Fig. 1. Interestingly there is a good agreement with those found by fitting the total energy [21]. The bond integrals obtained by Liu et al. [17] used a power law decay, which results in longer ranged bond integrals. However, around the equilibrium bond distance in

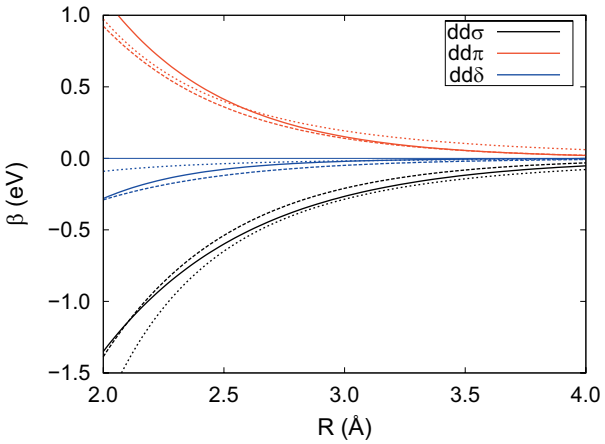

Figure 1 (online colour at: www.pss-b.com) Comparison of the bond integrals for the Fe–Fe bond. Solid lines: Madsen et al. [16], dashed lines: Paxton and Elsässer [21], dotted lines: Liu et al. [17]

solid Fe (≈2.5 Å) there is a fair agreement between the three parameterizations and, furthermore, the relative strength of the bond integrals shows a very good agreement with the canonical d-band ratio of −6:4:−1 [22].

For a close-packed solid with a nearest-neighbour distance of 2.5 Å, a rectangular d-band model [23] with these bond integrals leads to a root mean square band width of

$$W = 12\sqrt{\frac{|\beta_{\mathrm{dd}\sigma}| + 2|\beta_{\mathrm{dd}\pi}| + 2|\beta_{\mathrm{dd}\delta}|}{5}} = 6.8\ \mathrm{eV}. \qquad (7)$$

The density of states for fcc iron obtained with DFT and the TB model is compared in Fig. 2 and shows a good agreement with this simple prediction. Furthermore it is seen that there is a good agreement between DFT and TB. The main differences lie at 1.5 and 4.5 eV below the Fermi level, as the sd-hybridization is not accounted for in the model.

2.2 Repulsive and embedding potential The second term in Eq. (1) is a pair-wise repulsive contribution modelling the double counting term of the d electrons and the screened interaction of the ionic cores [11]. We write the repulsive potential as a simple exponential

$$E_{\mathrm{rep}} = \sum_{I,J\neq I} a_{\mathrm{rep}} \exp\left(-b_{\mathrm{rep}} R_{IJ}\right). \qquad (8)$$

We further approximate the contribution of the s-electrons to the cohesive energy in Eq. (1) with a simple embedding term. Based on the second-moment approximation to the density of states, we model the embedding term as having a square-root dependence on the coordination number [24, 25],

$$E_{\mathrm{emb}} = -\sum_{I} \left(\sum_{J\neq I} (a_{\mathrm{emb}})^2 \exp\left(-b_{\mathrm{emb}} R_{IJ}^2\right) \right)^{1/2}. \qquad (9)$$

For the embedding function we use a Gaussian-like radial dependence. For the repulsive and embedding terms, Eqs. (8) and (9), the exponents are fixed by the extracted bond and overlap integrals. The repulsive part we see as an overlap repulsion which should thus be proportional to the square of the most long-ranged dd-overlap integral. The embedding part we see as arising from not including the s-states in the bonding term, it is thus written in terms of the square of the $\beta_{\mathrm{ss}\sigma}$ matrix element for the Fe_2 dimer. We thus end up with a TB model where only two parameters must be found by fitting total energies. We fit the parameters a_{rep} and a_{emb}, Eqs. (8) and (9), to the DFT energy–volume curves for non-magnetic bcc, fcc and hcp structures.

2.3 The A15 structure We apply the TB model to the A15 (β-W or Cr_3Si) structure [26, 27]. The A15 structure has two symmetry-independent sites, one 12-fold coordinated and one 14-fold coordinated, see Fig. 3. The 14-fold coordinated site has two bonds which are substantially shorter than the twelve others. We have performed calculations in a unit cell with $a = 4.378$ Å, which means that the 12-fold coordinated site has the same bond lengths as the above mentioned fcc structure. The DOS for A15 iron obtained with DFT and the TB model is shown in Fig. 4. The positions of the main peaks are in good agreement.

3 Bond-order potentials The tight-binding model presented in the previous section may be used in simulations of up to a few hundred or a few thousand atoms. Then

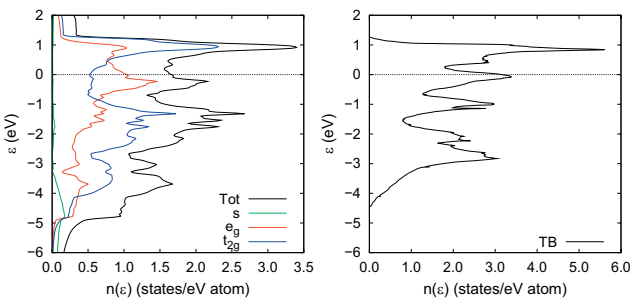

Figure 2 (online colour at: www.pss-b.com) Density of states of fcc-Fe calculated with DFT (left) and TB (right).

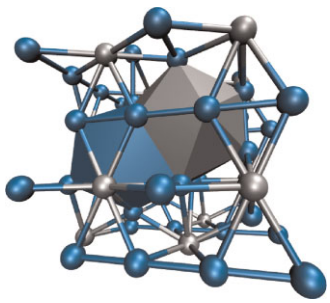

Figure 3 (online colour at: www.pss-b.com) Coordination polyhedra of the A15 structure.

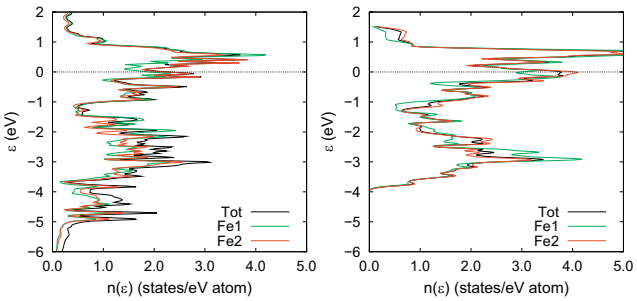

Figure 4 (online colour at: www.pss-b.com) Density of states of A15-Fe calculated with DFT (left) and TB (right).

standard diagonalization routines are not useful any longer but linear scaling approaches should be used. Linear scaling requires a local characterization of the electronic structure, which is a central focus of the bond-order potentials [12, 28–30]. By using Lanczos recursion [31, 32] and a continued fraction expansion of the local density of states, the *numerical* BOPs provide a linear scaling approximation to tight-binding [33–35], while the focus of the *analytic* BOPs is on the systematic derivation of interatomic potentials for semiconductors [36–38] and transition metals [39]. The BOPs use the moments theorem [40] to relate the atomic structure to the electronic structure,

$$\begin{aligned}\mu_{Iv}^{(n)} &= \int E^n n_{Iv}(E)\mathrm{d}E = \langle\varphi_{Iv}|\hat{H}^n|\varphi_{Iv}\rangle \\ &= \sum_{J\mu K\tau\cdots} H_{Iv J\mu}H_{J\mu K\tau}H_{K\tau\ldots}\cdots H_{\ldots Iv},\end{aligned} \tag{10}$$

where $H_{Iv J\mu}$ correspond to the TB matrix elements of Section 2 and the local density of states of the orthogonal TB model is given by

$$n_{Iv}(E) = \sum_k |c_{Iv}^{(k)}|^2\delta(E-E_k), \tag{11}$$

with the eigenvalues E_k and the expansion coefficients of the eigenstates ψ_k in the atomic basis, $c_{Iv}^{(k)} = \langle\varphi_{Iv}|\psi_k\rangle$. Analytic BOPs for transition metals are then obtained by approximating the local density of states by Chebyshev polynomials of the second kind,

$$n_{Iv}(\varepsilon) = \frac{2}{\pi}\sqrt{1-\varepsilon^2}\left[1+\sum_{n=1}\sigma_n U_n(\varepsilon)\right], \tag{12}$$

where the energy $\varepsilon = (E-a_\infty)/(2b_\infty)$ has been centred and rescaled with the parameters a_∞ and b_∞ such that the eigenspectrum is contained in the interval $[-1, 1]$. As the Chebyshev polynomials $U_n = \sum_{k=0}^n p_{nk}\varepsilon^k$ are orthogonal, the expansion coefficients σ_n may be obtained by projection,

$$\sigma_n = \int U_n(\varepsilon)n_{Iv}(\varepsilon)\mathrm{d}\varepsilon = \sum_{k=0}^n p_{nk}\hat{\mu}_{Iv}^{(k)}, \tag{13}$$

where the moments $\hat{\mu}_{Iv}^{(n)}$ were adapted to the energy scale ε. Equation (12) may be integrated analytically, resulting in analytic expressions for the number of electrons and the bond energy:

$$N_{Iv}(\phi_\mathrm{F}) = \sum_n \sigma_n\hat{\chi}_{n+1}(\phi_\mathrm{F}), \tag{14}$$

$$E_{\mathrm{bond},Iv} = b_\infty\sum_n\sigma_n[\hat{\chi}_{n+2}(\phi_\mathrm{F})-\gamma_0\hat{\chi}_{n+1}(\phi_\mathrm{F})+\hat{\chi}_n(\phi_\mathrm{F})], \tag{15}$$

with the response functions

$$\hat{\chi}_n(\phi_\mathrm{F}) = \frac{1}{\pi}\left(\frac{\sin(n+1)\phi_\mathrm{F}}{n+1}-\frac{\sin(n-1)\phi_\mathrm{F}}{n-1}\right) \tag{16}$$

for $n>1$, the Fermi energy $\varepsilon_\mathrm{F} = \cos(\phi_\mathrm{F})$ and $\gamma_0 = \sigma_1$. A similar expansion of the bond order/density matrix results in an explicit analytic expression of the bond order [39].

3.1 Molecular dynamics simulations with analytic BOPs We applied the analytic BOPs as implemented in BOPfox [41] for the simulation of topologically close-packed (tcp) phases [26, 42]. The tcp phases are of technological relevance, for example, in Nickel-based superalloys [43] or precipitation hardened steels. The structural complexity of the tcp phases prohibits a description with simple interatomic potentials, while atomistic calculations with simple TB and BOP models [44] were shown to capture the trend of structural stability of tcp phases predicted by ab initio calculations [45].

Here, we demonstrate that the BOPs open the way also for dynamic simulations of tcp phases. We focus on the A15 (β-W) phase (cf. Fig. 3), as tungsten is one of the elements where a tcp phase is observed and found to be metastable [46]. Our BOP simulations employ a simple model developed by Lim [47]. We include six moments to approximate the TB density of states in our BOP calculations and assume local charge neutrality. The numerical values of a_∞ and b_∞ are set to the lowest recursion-coefficients of the ideal A15 phase.

We carried out MD simulations for 10 000 steps using a velocity-Verlet integrator with a 1 fs time-step. In order to investigate the temperature-dependence of the structural stability of the A15 phase within our model, we carried out a series of calculations at different system temperatures adjusted by the Andersen thermostat [48]. The radial distribution function (RDF) is shown in Fig. 5 for different temperatures. The radii in the ideal neighbour shells (peaks shown for 0 K) are smeared out already at a temperature of 100 K, but several individual peaks of the first four neighbour shells are still visible. The reduced separation of the shells with increasing temperature indicates the onset of structural deformations. Therefore, we conclude that with the employed BOP model and up to six moments taken into account in the analytic BOP expansion, the A15 structure is mechanically stable for small temperatures. As a first step towards simulating tcp phase precipitation, we constructed an interface between the metastable A15 phase and the bcc

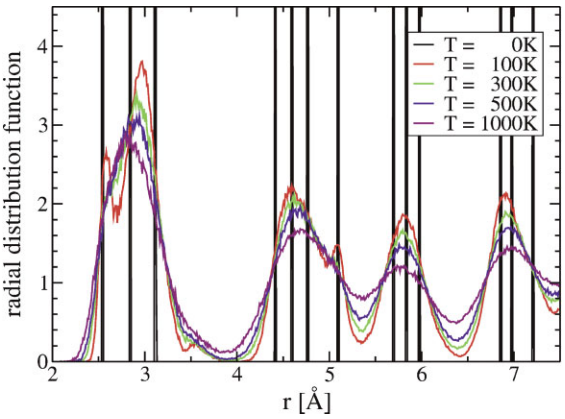

Figure 5 (online colour at: www.pss-b.com) A15 phase: radial-distribution function at different temperatures.

ground-state phase of W by connecting a $6 \times 6 \times 6$ repetition of a cubic bcc unit cell with a $4 \times 4 \times 4$ repetition of a cubic A15 unit cell in the (100) plane. In order to match the two phases within the simulation cell (Fig. 6), we needed to apply compressive strain (-4%) to the A15 structure and tensile strain ($+2\%$) to the bcc structure. We also introduced vacancies in the A15 structure in order to match the number of atoms in either half which resulted in 864 atoms in total. This initial interface structure was relaxed with a conjugate-gradient algorithm and then used in MD simulations in order to investigate the structural stability of the interface structure at elevated temperature. The MD simulations were carried out at a temperature of 700 K and 50 000 MD steps of 1 fs each. The bcc/A15 environment that is clearly visible in the interface structure after relaxation (Fig. 6, left) undergoes strong structural changes in the A15 part during the MD simulation (Fig. 6, right). The bcc part on the other hand preserves its atomic structure.

4 Extended time scale simulations While the system size and simulation time is increased considerably by going from DFT to a coarse-grained description of the electronic structure in TB or BOPs, the maximum time step, Δt, within a MD simulations is still determined by the fastest motion in the system. The fastest motion in a solid are usually vibrations with a period of a few hundred femto seconds, i.e. to resolve the vibrations Δt has to be on the order of a few femto seconds. Even with the fastest empirical potentials simulation times nowadays only reach up to microseconds, which is often much to short for the calculation of the thermodynamic or kinetic behaviour of materials.

If the long time behaviour within a system is dominated by so-called *rare events*, much longer simulation times of up to minutes or hours are necessary. Rare events, in this context, are characterized by transitions between local minima in the potential energy surface that are separated by comparably high free energy barriers, such that there is a separation of time scales between the short time dynamics within the local minima (vibrations, fs) and the transitions between them (diffusion, structural rearrangements, ns. . .s). Therefore, if it is possible to properly extract the time evolution of the rare events based on the underlying atomistic dynamics, much longer time scales can be reached while still retaining atomistic detail in the simulations.

Various methods have been developed to sample rare events and to follow the corresponding state-to-state dynamics over extended time scales, including umbrella sampling [49], blue moon sampling [50], transition path sampling [51], metadynamics [52] and the accelerated molecular dynamics techniques [53]. Here, we focus on the kinetic Monte Carlo [54–58] approach where the transition between stable system states is described by a Markov chain and the atomic short time dynamics is appropriately averaged into the transition probabilities.

4.1 Adaptive kinetic Monte Carlo The major challenge in performing kinetic Monte Carlo simulations is the setup of an adequate model. This requires a suitable decomposition of state space, the definition of stable states in configuration space and an accurate determination of transition probabilities. If the decomposition of state space is known, the stable states can be mapped onto a lattice and all transition probabilities can be calculated and tabulated in advance, allowing for a fast and efficient numerical evaluation. If, on the other hand, the dynamics are dominated by non-intuitive events which cannot simply be guessed, a lattice kMC model is unfeasible. In such a case, the important transition processes have to be identified on-the-fly during the simulation in an adaptive kMC approach [59]. Assuming that the transition rate constants from a state A to a state B, $k_{\mathrm{A}\to\mathrm{B}}$, can be calculated employing harmonic transition state theory (hTST) [60],

$$k_{\mathrm{A}\to\mathrm{B}}^{\mathrm{hTST}} = \frac{\prod_{i}^{N} \nu_i^{\mathrm{A}}}{\prod_{i}^{N-1} \nu_i^{\mathrm{TS}}} \exp\left(-\frac{\Delta E}{k_{\mathrm{B}} T}\right), \tag{17}$$

with ν_i the vibrational frequencies in the initial state A and at the transition state TS, ΔE the energy difference between A and TS, k_{B} the Boltzmann constant and T the temperature, the problem is reduced to finding the saddle points around a specific minimum which mark the transition states for all relevant escape paths. Within the akMC approach the saddle point search is performed by the dimer method [61], a minimum-mode following method requiring only infor-

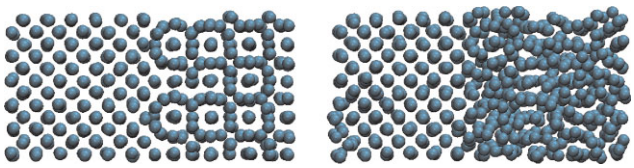

Figure 6 (online colour at: www.pss-b.com) bcc-A15 interface: initial relaxed atomic structure (left) and after MD simulation (right).

mation about the initial state. Alternatively, the lowest curvature can be determined using the Lagrange multiplier [62] or the Lanczos method [63]. After all relevant escape paths have been identified a rate constant table is setup using Eq. (17), an escape path is chosen randomly but correctly weighted, and the system is moved into the next state. Within the new state again saddle point searches are performed to find the corresponding escape processes. Since typically only a few hundred force calls are needed for the saddle point searches within the dimer method, it is even feasible to carry out akMC simulations based on DFT [64].

4.2 Correlated hydrogen and vacancy diffusion in Fe Diffusion is a classical rare event problem. Very often the atomic rearrangements during diffusion are relativley simple and can suitably be described within a lattice kMC model. If, for example, several point defects are involved or if several atomic displacements are correlated such as to preserve the long-range order of an alloy, the situation becomes more complicated and diffusion processes can also include the concerted motion of several atoms.

As an example we discuss the diffusion of hydrogen atoms in the vicinity of a vacancy in bcc-Fe. Hydrogen prefers the tetrahedral interstitial site in bcc-Fe, and shows a rather low solubility and a very high mobility. Vacancies and other point defects provide trapping sites, considerably lowering the dissolution energy of hydrogen. Due to the fast diffusion in the bulk and trapping at defect sites, already small volume concentrations of hydrogen can significantly influence the materials properties.

In an atomistic study of the diffusion of hydrogen in the presence of vacancies that was based on a sophisticated kMC model [65], it was found that the calculated effective diffusion constants showed discrepancies as compared to trapping theory [66]. This was attributed to a poor evaluation of diffusion barriers close to the vacancies within the employed embedded atom method potential, emphasizing the importance of an accurate description of the atomic interactions. Using DFT it was shown that the binding of up to two H atoms to a vacancy (Va) is exothermic and that predominantly VaH_2 clusters form [67, 68]. The formation energy of a VaH_2 complex is lower than the formation energy of a single vacancy, indicating that the presence of hydrogen may enhance the formation of vacancies. Furthermore, hydrogen atoms induce an anisotropy in the clustering of vacancies. In a recent DFT study [69] hydrogen-vacancy interaction in the presence of carbon was investigated. The binding process is dominated by Va-H and Va-C interactions leading to an effective decoupling of Va_xC_y and Va_xH_z clusters. The mobility of such clusters has not been investigated in detail on an atomistic level, but it was suggested that small Va-H clusters might be highly mobile and could thus contribute to the diffusion of vacancies to extended defects such as dislocations or grain boundaries.

As a first step towards investigating the mobility of Va-H clusters we study a $(2 \times 2 \times 2)$ cell in bcc-Fe containing one vacancy and one hydrogen atom as shown in Fig. 7. In order

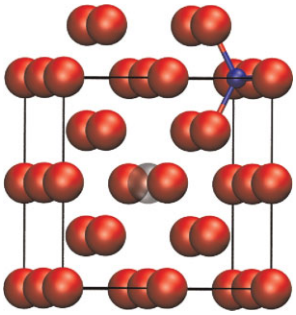

Figure 7 (online colour at: www.pss-b.com) Initial setup for hydrogen/vacancy diffusion in bcc Fe. Red, large spheres denote Fe atoms, small, blue sphere denotes the H atom and the transparent sphere marks the vacancy.

to obtain the state-to-state trajectory we employ an akMC approach based on DFT. All calculations are performed within the projector augmented-wave method [70, 71] as implemented in the VASP code [72, 73], the generalized gradient approximation (PW91) [74] was used for the exchange correlation functional. The energy cutoff for the plane waves was 280 eV and the integration of the Brillouin zone was done on a $[4 \times 4 \times 4]$ grid within the Monkhorst–Pack scheme [75]. All calculations included spin-polarization. This rather moderate basis set allows for a fast evaluation of energies and forces with reasonable accuracy. The akMC simulations were carried out using the VASP transition state theory tools [76]. As in the present study the focus is on finding potentially correlated diffusion mechanisms and not on the quantitative prediction of diffusion coefficients, we did not calculate the prefactor in Eq. (17) explicitly but kept it at a fixed value of $\nu_0 = \prod_i^n \nu_i^{\mathrm{A}} / \prod_i^{N-1} \nu_i^{\mathrm{TS}} = 10^{12}\ \mathrm{s}^{-1}$, the temperature was set to $T = 300\,\mathrm{K}$. Better agreement with experiment is reached if ν_0 is calculated explicitly [65, 77]. We furthermore did not correct the migration barriers for quantum mechanical contributions such as the zero point energy which significantly alter the migration energy of hydrogen [77, 78] or finite temperature corrections such as spin fluctuations but obtained the migration energies from a zero-temperature analysis based on a classical Born–Oppenheimer separation of nuclear and electronic degrees of freedom.

During the akMC simulations all single atom hop diffusion processes that had been suggested previously were found automatically by the saddle point search algorithm. These include: (1) A hop of a hydrogen atom between two neighbouring tetrahedral sites with a barrier of $\Delta E = 0.1\,\mathrm{eV}$. (2) A hydrogen atom hopping from a bulk tetrahedral site into a vacancy site, $\Delta E = 0.07\,\mathrm{eV}$, and the reverse process, $\Delta E = 0.58\,\mathrm{eV}$. Each vacancy site has four neighbouring tetrahedral bulk sites. (3) Diffusion of hydrogen atoms within the vacancy, $\Delta E = 0.18\,\mathrm{eV}$. There are six binding sites for H atoms within the vacancy, diffusion occurs between a binding site and one of its four neighbouring sites. (4) Vacancy diffusion, i.e. one of the nearest neighbour Fe atoms hops into the vacancy,

Table 1 Energy barriers for diffusion processes of hydrogen and vacancies in bcc-Fe found during the akMC simulation. All values are given in eV.

single atom hop	
$H_{T\text{-site}} \leftrightarrow H_{T\text{-site}}$	0.10
$H_{T\text{-site}} \leftrightarrow H_{Va\text{-site}}$	0.07/0.58
$H_{Va\text{-site}} \leftrightarrow H_{Va\text{-site}}$	0.18
$Va \leftrightarrow Va$	0.68
concerted moves	
$Va + H_{T\text{-site}} \leftrightarrow Va + H_{Va\text{-site}}$	0.36/0.87 0.63/1.13

$\Delta E = 0.68$ eV. These results compare well with previous DFT studies [65, 77–80]. The diffusion barriers are summarized in Table 1. It should, however, be pointed out that the vacancy migration energy predicted by DFT is in conflict with experimental data [81]. An analysis of this discrepancy is beyond the scope of the present paper but must be resolved before a quantiative comparison between experiment and theory will be possible.

In addition to the four single atom hop processes, two concerted moves were found in the akMC simulations. In both cases the hydrogen atom sits in a tetrahedral site and moves together with an iron atom ending up in a vacancy site, such that both the H atom and the vacancy have moved as shown in Fig. 8. In the diffusion process depicted in the upper part of Fig. 8 the H and Fe atom move into the same direction with a relatively low barrier of $\Delta E = 0.36$ eV. In the second concerted motion the H and Fe atom move into opposite direction with a higher barrier of $\Delta E = 0.63$ eV. It should be noted that both barriers for the concerted H/Fe diffusion processes are lower than the barrier for a simple vacancy diffusion. Especially, with respect to the low barrier concerted process, the presence of hydrogen significantly facilitates the diffusion of a vacancy.

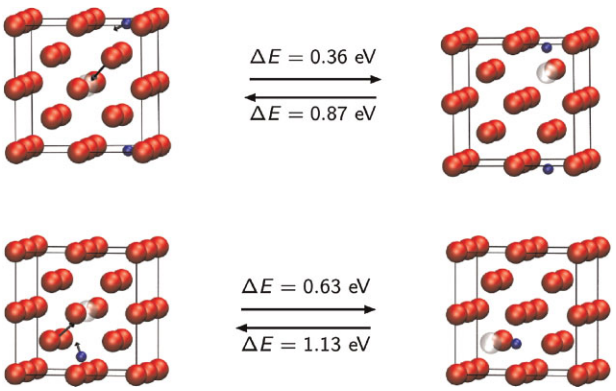

Figure 8 (online colour at: www.pss-b.com) Concerted diffusion processes of hydrogen and iron atoms in bcc-Fe. In the upper figure both the H and Fe atom move into the same direction, whereas in the lower figure they move into opposite directions leading to a higher diffusion barrier. In both cases the H atom is initially in a tetrahedral site and moves to a vacancy site.

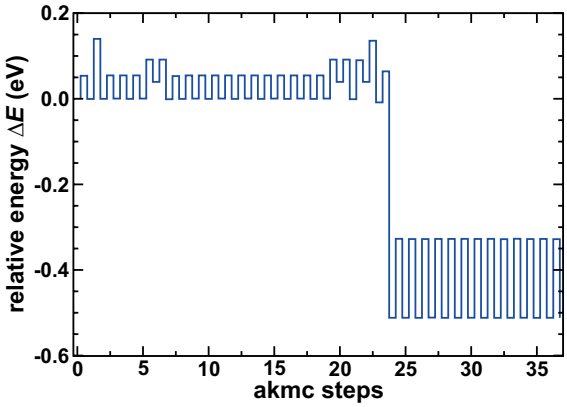

Figure 9 (online colour at: www.pss-b.com) Energy profile of a typical akMC trajectory. The energy is given relative to a hydrogen atom in a tetrahedral site. The hydrogen atom first moves between different tetrahedral sites before it binds to the vacancy. Trapped inside the vacancy the hydrogen atom diffuses between the different binding sites within the vacancy.

The energy profile of a typical trajectory of the akMC run is shown in Fig. 9. The energy is given with respect to a hydrogen atom in a tetrahedral site. Starting from the configuration shown in Fig. 7, the hydrogen atom diffuses between different tetrahedral sites with a very low diffusion barrier before it binds to the vacancy and is trapped there (by about 0.5 eV), moving around the different binding sites within the vacancy. The total time of the shown trajectory is ~4 ns. Due to the very large escape barrier of 0.6 eV, the probability for the H atom to leave the vacancy is extremely low and was not observed at $T = 300$ K, but in simulations with $T = 600$ K.

Our simulations showed that even in this relatively simple setup there exist concerted diffusion processes that exhibit lower barriers than the corresponding single atom hop processes. To investigate the implications for the diffusion of hydrogen-vacancy clusters, larger supercells with more hydrogen atoms and more vacancies are necessary. We are currently investigating the behaviour of several H atoms within a $(3 \times 3 \times 3)$ supercell. Based on DFT, these simulations require a significant computational cost, highlighting again the importance of fast and reliable TB models and BOPs to be able to go to large system sizes.

5 Conclusion and outlook In our contribution to this special issue we discussed how a coherent link from the electronic to the microstructural modelling hierarchies may be established from DFT to TB, BOPs and akMC. Because of a systematic and physically transparent coarse graining at each of the three levels of approximation, an intuitive interpretation of the electronic structure in TB, of the interatomic interaction in BOPs and the events observed in akMC is possible. As no underlying lattice is required for the simulations, the methodology presented in this contribution may be applied to investigate a priori unknown materials behaviour. This is relevant in particular for technologically

important materials such as steels or superalloys where the unexpected formation of new phases during service was observed or the role of the various constituents in hydrogen embrittlement is unclear.

Furthermore, the atomistic simulations presented in this paper provide the basis for microstructural simulations of materials properties. Phase field simulations that model the phase transformation kinetics in solidification may benefit from effective interface energies and relative phase stabilites obtained in atomistic simulations, while micromechanical simulation of the plastic deformation of a material require a detailed knowledge of dislocation and grain boundary properties, which are accessible with the methods presented in this contribution.

Acknowledgements The authors acknowledge financial support through ThyssenKrupp AG, Bayer MaterialScience AG, Salzgitter Mannesmann Forschung GmbH, Robert Bosch GmbH, Benteler Stahl/Rohr GmbH, Bayer Technology Services GmbH and the state of North-Rhine Westphalia as well as the EU in the framework of the ERDF.

References

[1] M. Fähnle, R. Drautz, F. Lechermann, R. Singer, A. Diaz-Ortiz, and H. Dosch, Phys. Status Solidi B **242**, 1159 (2005).
[2] J. Sanchez, F. Ducastelle, and D. Gratias, Physica A **128**, 334 (1984).
[3] R. Drautz, H. Reichert, M. Fähnle, H. Dosch, and J. M. Sanchez, Phys. Rev. Lett. **87**(23), 236102 (2001).
[4] R. Drautz, A. Díaz-Ortiz, M. Fähnle, and H. Dosch, Phys. Rev. Lett. **93**(6), 067202 (2004).
[5] R. Drautz, R. Singer, and M. Fähnle, Phys. Rev. B **67**(3), 035418 (2003).
[6] F. Lechermann, M. Fähnle, and J. Sanchez, Intermetallics **13**, 1096 (2005).
[7] R. Drautz, M. Fähnle, and J. M. Sanchez, J. Phys.: Condens. Matter **16**, 3843 (2004).
[8] G. Bester and M. Fähnle, J. Phys.: Condens. Matter **13**, 11541 (2001).
[9] N. Börnsen, G. Bester, B. Meyer, and M. Fähnle, J. Alloys Compd. **308**, 1 (2000).
[10] W. Kohn and L. J. Sham, Phys. Rev. A **140**, 1133 (1965).
[11] A. P. Sutton, M. W. Finnis, D. G. Pettifor, and Y. Ohta, J. Phys. C, Solid State Phys. **21**, 35 (1988).
[12] M. Finnis, Interatomic Forces in Condensed Matter (Oxford University Press, Oxford, 2003).
[13] M. W. Finnis, J. Phys.: Condens. Matter **2**(2), 331 (1990).
[14] M. Elstner, D. Porezag, G. Jungnickel, J. Elsner, M. Haugk, T. Frauenheim, S. Suhai, and G. Seifert, Phys. Rev. B **58**, 7260 (1998).
[15] M. W. Finnis, A. T. Paxton, M. Methfessel, and M. van Schilfgaarde, Phys. Rev. Lett. **81**(23), 5149 (1998).
[16] G. K. H. Madsen, E. J. McEniry, and R. Drautz, Phys. Rev. B **83**, 184119 (2011).
[17] G. Liu, D. Nguyen-Manh, B. G. Liu, and D. G. Pettifor, Phys. Rev. B **71**, 174115 (2005).
[18] N. Börnsen, B. Meyer, O. Grother, and M. Fähnle, J. Phys.: Condens. Matter **11**, L287 (1999).
[19] A. Urban, M. Reese, M. Mrovec, C. Elsässer, and B. Meyer, (2010), submitted.
[20] J. C. Slater and G. F. Koster, Phys. Rev. **94**(6), 1498 (1954).
[21] T. Paxton and C. Elsässer, Phys. Rev. B **82**, 235125 (2010).
[22] O. K. Andersen, Solid State Commun. **13**, 133 (1973).
[23] D. G. Pettifor, Bonding and Structure of Molecules and Solids (Clarendon Press, Oxford, UK, 1995).
[24] F. Ducastelle and F. Cyrot-Lackmann, J. Phys. Chem. Solids **31**, 1295 (1970).
[25] G. Allen and M. Lannoo, J. Phys. Chem. Solids **37**, 699 (1976).
[26] A. K. Sinha, Prog. Mater. Sci. **15**, 79 (1973).
[27] P. Turchi, G. Treglia, and F. Ducastelle, J. Phys. F, Met. Phys. **13**, 2543 (1983).
[28] D. G. Pettifor, Phys. Rev. B **63**, 2480 (1989).
[29] M. W. Finnis, Prog. Mater. Sci. **52**, 133 (2007).
[30] T. Hammerschmidt, R. Drautz, and D. G. Pettifor, Int. J. Mater. Sci. **100**, 1479 (2009).
[31] C. Lanczos, J. Res. Natl. Bur. Stand. **45**, 225 (1950).
[32] R. Haydock, Recursive Solution of Schrödinger's Equation, in: Solid State Physics, edited by H. Ehrenreich, F. Seitz, and D. Turnbull (Academic, New York, 1980), p. 215.
[33] M. Aoki, Phys. Rev. Lett. **71**, 3842 (1993).
[34] A. Horsfield, A. M. Bratkovsky, M. Fearn, D. G. Pettifor, and M. Aoki, Phys. Rev. B **53**, 12694 (1996).
[35] M. Aoki, D. Nguyen-Manh, D. G. Pettifor, and V. Vitek, Prog. Mater. Sci. **52**, 154 (2007).
[36] D. G. Pettifor and I. I. Oleinik, Phys. Rev. B **59**, 8487 (1999).
[37] R. Drautz, X. W. Zhou, D. A. Murdick, B. Gillespie, H. N. G. Wadley, and D. G. Pettifor, Prog. Mater. Sci. **52**, 196 (2007).
[38] M. Mrovec, M. Moseler, C. Elsässer, and P. Gumbsch, Prog. Mater. Sci. **52**, 230 (2007).
[39] R. Drautz and D. G. Pettifor, Phys. Rev. B **74**, 174117 (2006).
[40] F. Cryot-Lackmann, Adv. Phys. **16**, 393 (1967).
[41] T. Hammerschmidt, B. Seiser, M. E. Ford, D. G. Pettifor, and R. Drautz, BOPfox program for tight-binding and bond-order potential calculations, unpublished.
[42] B. Seiser, R. Drautz, and D. Pettifor, Acta Mater. **59**, 749 (2011).
[43] C. M. F. Rae and R. C. Reed, Acta Mater. **49**, 4113 (2001).
[44] T. Hammerschmidt, B. Seiser, R. Drautz, and D. G. Pettifor, Modelling topologically close-packed phases in superalloys: Valence-dependent bond-order potentials based on ab-initio calculations, in: Superalloys 2008, edited by R. C. Reed, K. Green, P. Caron, T. Gabb, M. Fahrmann, E. Huron, and S. Woodward (The Metals, Minerals and Materials Society, Warrendale, PA, USA, 2008), p. 847.
[45] C. Berne, A. Pasturel, M. Sluiter, and B. Vinet, Phys. Rev. Lett. **83**, 1621 (1999).
[46] W. Morcom, W. Worrcell, H. Sell, and H. Kaplan, Metall. Trans. **5**(1), 155 (1974).
[47] H. Lim, PhD thesis, University of Oxford (1992).
[48] H. Andersen, J. Chem. Phys. **72**(4), 2384 (1980).
[49] G. M. Torrie and J. P. Valleau, Chem. Phys. Lett. **28**(4), 578 (1974).
[50] E. Carter, G. Ciccotti, J. T. Hynes, and R. Kapral, Chem. Phys. Lett. **156**(5), 472 (1989).
[51] C. Dellago, P. G. Bolhuis, and P. L. Geissler, Adv. Chem. Phys. **123**, 1 (2002).
[52] A. Laio and M. Parrinello, Proc. Natl. Acad. Sci. USA **99**(20), 12562 (2002).
[53] A. F. Voter, F. Montalenti, and T. C. Germann, Annu. Rev. Mater. Res. **32**, 321 (2002).

[54] A. B. Bortz, M. H. Kalos, and J. L. Lebowitz, J. Comput. Phys. **17**, 10 (1975).
[55] D. T. Gillespie, J. Comput. Phys. **22**, 403 (1976).
[56] A. F. Voter, Phys. Rev. B **34**(10), 6819 (1986).
[57] H. C. Kang and W. H. Weinberg, J. Chem. Phys. **90**(5), 2824 (1989).
[58] K. A. Fichthorn and W. H. Weinberg, J. Chem. Phys. **95**(2), 1090 (1991).
[59] G. Henkelman and H. Jónsson, J. Chem. Phys. **115**(21), 9657 (2001).
[60] G. H. Vineyard, J. Phys. Chem. Solids **3**, 121 (1957).
[61] G. Henkelman and H. Jónsson, J. Chem. Phys. **111**(15), 7010 (1999).
[62] L. J. Munro and D. J. Wales, Phys. Rev. B **59**(6), 3969 (1999).
[63] R. Malek and N. Mousseau, Phys. Rev. E **62**(6), 7723 (2000).
[64] L. Xu and G. Henkelman, J. Chem. Phys. **129**(11), 114104 (2008).
[65] A. Ramasubramaniam, M. Itakura, M. Oritz, and E. A. Carter, J. Mater. Res. **23**(10), 2757 (2008).
[66] R. Oriani, Acta Metall. **18**(1), 147 (1970).
[67] Y. Tateyama and T. Ohno, Phys. Rev. B **67**(17), 174105 (2003).
[68] Y. Tateyama and T. Ohno, ISIJ Int. **43**(4), 573 (2003).
[69] P. R. Monasterio, T. T. Lau, S. Yip, and K. J. Van Vliet, Phys. Rev. Lett. **103**(8), 085501 (2009).
[70] P. E. Blöchl, Phys. Rev. B **50**(24), 17953 (1994).
[71] G. Kresse and D. Joubert, Phys. Rev. B **59**(3), 1758 (1999).
[72] G. Kresse and J. Hafner, Phys. Rev. B **47**(1), 558 (1993).
[73] G. Kresse and J. Furthmüller, Phys. Rev. B **54**(16), 11169 (1996).
[74] J. P. Perdew, J. A. Chevary, S. H. Vosko, K. A. Jackson, M. R. Pederson, D. J. Singh, and C. Fiolhais, Phys. Rev. B **46**(11), 6671 (1992).
[75] H. J. Monkhorst and J. D. Pack, Phys. Rev. B **13**(12), 5188 (1976).
[76] http://theory.cm.utexas.edu/vtsttools/akmc/.
[77] D. E. Jiang and E. A. Carter, Phys. Rev. B **70**(6), 064102 (2004).
[78] J. Sanchez, J. Fullea, C. Andrade, and P. L. de Andres, Phys. Rev. B **78**, 014113 (2008).
[79] C. Domain and C. S. Becquart, Phys. Rev. B **65**(2), 024103 (2001).
[80] C. C. Fu, J. Dalla Torre, F. Williame, J. L. Boquet, and A. Barbu, Nature Mater. **4**, 68 (2005).
[81] A. Seeger, Phys. Status Solidi A **167**, 289 (1998).